Atmos. Chem. Phys. Discuss., 13, 10009–10047, 2013
www.atmos-chem-phys-discuss.net/13/10009/2013/
doi:10.5194/acpd-13-10009-2013

Atmospheric Chemistry and Physics Discussions

Frequency of deep convective clouds in the tropical zone from ten years of AIRS data

H. H. Aumann and A. Ruzmaikin

California Institute of Technology, Jet Propulsion Laboratory, Pasadena CA, USA

Received: 2 February 2013 – Accepted: 1 April 2013 – Published: 17 April 2013

Correspondence to: H. H. Aumann (aumann@jpl.nasa.gov)

Published by Copernicus Publications on behalf of the European Geosciences Union.

Abstract

Deep Convective Clouds (DCC) have been widely studied because of their association with heavy precipitation and severe weather events. To identify DCC with Atmospheric Infrared Sounder (AIRS) data we use three types of thresholds: (1) thresholds based on the absolute value of an atmospheric window channel brightness temperature; (2) thresholds based on the difference between the brightness temperature in an atmospheric window channel and the brightness temperature centered on a strong water vapor absorption line; and (3) a threshold using the difference between the window channel brightness temperature and the tropopause temperature based on climatology. We find that DCC identified with threshold (2) (referred to as DCCw4) cover 0.16 % of the area of the tropical zone and 72 % of them are identified as deep convective, 39 % are overshooting based on simultaneous observations with the Advanced Microwave Sounding Unit-HSB (AMSU-HSB) 183 GHz water vapor channels. In the past ten years the frequency of occurrence of DCC decreased for the tropical ocean, while it increased for tropical land. The land increase-ocean decrease closely balance, such that the DCC frequency changed at an insignificant rate for the entire tropical zone. This pattern of essentially zero trend for the tropical zone, but opposite land/ocean trends, is consistent with measurements of global precipitation. The changes in frequency of occurrence of the DCC are correlated with the Niño34 index, which defines the SST anomaly in the East-Central Pacific. This is also consistent with patterns seen in global precipitation. This suggests that the observed changes in the frequency are part of a decadal variability characterized by shifts in the main tropical circulation patterns, which does not fully balance in the ten year AIRS data record. The regional correlations and anti-correlations of the DCC frequency anomaly with the Multivariate ENSO Index (MEI) provides a new perspective for the regional analysis of past events, since the SST anomaly in the Nino34 region is available in the form of the extended MEI since 1871. Depending on the selected threshold, the frequency of DCC in the tropical zone ranges from 0.06 % to 0.8 % of the area. We find that the least frequent, more

ACPD
13, 10009–10047, 2013

extreme DCC also show the largest trend in frequency, increasing over land, decreasing over ocean. This finding fits into the framework of how weather extremes respond to climate change.

1 Introduction

Extremely cold deep convective clouds are frequently associated with severe weather and heavy precipitation events. A detection of a trend in the frequency of these clouds would have significant implication on our understanding of changes in the frequency of severe storms. However, while there are many papers on deep convective clouds, no studies of trends in frequency of deep convective clouds are found in the literature.

The association between severe weather and extremely cold clouds was first noted in 11 µm images from Earth orbiting satellites three decades ago (Adler et al., 1979; Reynolds, 1980). The association between heavy rainfall and deep convective clouds has led to the development of a precipitation algorithm for GOES (Janowiak and Arkin, 1991; Joyce and Arkin, 1997). Cases where the brightness temperatures at 6.7 µm is warmer than at 11 µm (e.g. Ackerman, 1996; Schmetz et al., 1997) were interpreted as convective overshooting clouds, providing further evidence of their association with deep convective storms. More recently, severe storms have been associated with the overshooting clouds, which are a subclass of DCC (e.g. Setvak et al., 2008; Bedka et al., 2010; Setvak et al., 2013). Damage associated with severe storm is well documented for relatively densely populated land areas. However, in the tropical zone, where severe storms are common, these events may be less striking and therefore less documented.

Satellite data have been used to identify DCC and cloud tops that reach or overshoot the Tropopause Transition Layer (TTL) (Fueglistaler et al., 2009; Gettleman et al., 2009), but these definitions are dependent on footprint size and the spectral channels available for the analysis. Thus Gettelman et al. (2002) selected DCC based on a brightness temperature in the 11um channel, $BT_{11} < 210$ K. These objects cover less

ACPD
13, 10009–10047, 2013

than 1 % of the tropical zone. They then identified those clouds that are colder than the temperature of the climatological tropopause (0.5 % of the tropical zone) as "overshooting convection". Alcala and Dessler (2002) and Liu and Zipser (2005, 2008) identified 20 DBZ Precipitation Features (PF) with the 13.8 GHz rain radar from TRMM (Tropical Rainfall Measuring Mission). Deep convection was associated with PF above the Level of Neutral Buoyancy (LNB) and overshooting convection was identified by PF where the associated height exceeds the climatological tropopause height. Hong et al. (2005) used a set of inequalities derived from 183 GHz sounder channels from AMSU-B (Advanced Microwave Sounding Unit) to identify 0.6 % of the area of the tropical zone as deep convective clouds. Young et al. (2012) used one year (2007) of TRMM 95 GHz space-borne cloud radar data, CloudSat data, and MODerate resolution Imaging Sounder (MODIS) data to show that 61 % of the Cold Cloud Features (CCF) identified by the condition $BT_{11} < 210$ K, cover about 1 % of the tropical zone and are associated with precipitation features from TRMM at higher than 14 km altitude, i.e. reach the bottom of the TTL.

The ability to detect these cold clouds in the infrared has been available for decades from the High Resolution Infrared Sounder (HIRS) and the Advanced Very High Resolution Radiometer (AVHRR). Wylie et al. (2005) published a study of trends in the frequency of high clouds using the IR data from a 25 yr long series of High Resolution Infrared Sounder (HIRS). The high clouds covered about 40 % of the area of the tropical zone, two orders of magnitude more than the frequency of DCC. He found no significant trends. In view of the association of DCC with heavy precipitation, the time series of tropical precipitation can be used as proxy for changes in the frequency of DCC. The WCRP report on Global Precipitation (2008) finds no significant trend in precipitation between 1979 and 2004.

The objective of our study is to use the first ten years of IR data from AIRS to evaluate trends in the frequency of DCC the tropical zone and to interpret the results using the correlation with the vertical pressure velocity at 500 hPa and the Nino34 index. In Sect. 2 we introduce the AIRS and AMSU-HSB data used in the analysis. In Sect. 3

ACPD
13, 10009–10047, 2013

we describe criteria for selecting DCC. Section 4 presents trend results. In Sect. 5 we analyze correlations between the DCC frequency, vertical velocity and the Nino34 index from a climate perspective.

2 Data

AIRS is uniquely suited for the detection of a change in the DCC frequency. AIRS (together with MODIS) has been in orbit for the past 10 yr with the expectation of a 20 yr lifetime. The AIRS absolute calibration accuracy and stability have been well documented (Aumann et al., 2007, 2012). AIRS was launched in May 2002 on the EOS Aqua satellite into a 705 km altitude sun-synchronous, 98° inclination circular orbit. We refer to the 1.30 p.m. ascending node as the "day" overpass, and to the 1.30 a.m. descending part of each orbit as the "night" overpass. The ascending node and altitude of the orbit are actively maintained. The AIRS footprint subtends an angle of 1.1°. The footprints are scanned ±49.5° cross-track resulting in a 1650 km wide swath. The footprint geometrical size on the ground increases from a spot of 13.5 km diameter at nadir to a 99 × 23 km ellipse at the extreme scan angles, with an average 30 km size averaged over all scan angles. On the same spacecraft as AIRS is the Humidity Sounder for Brazil (HSB) instrument (Lambrigtsen and Calheiros 2003). Since the HSB has the same channels at 183 GHz as AMSU-B on a number of NOAA spacecraft, we refer to HSB in the following simply as AMSU-HSB. It has the same 1.1° footprint size and scan pattern as AIRS. The AIRS and AMSU-HSB scan patterns are synchronized and their footprints are aligned to within 0.2° (Lambrigtsen and Lee, 2003). AIRS and AMSU-HSB thus provide essentially simultaneous coverage of infrared data with 183 GHz microwave data. The AMSU-HSB on EOS Aqua produced quality data only between 1 September 2002 and 4 February 2003.

Essentially un-interrupted AIRS data are available since 1 September 2002 to present. Each day, AIRS generates 3 million spectra, which are available from the GSFC/DISC in the form of 240 files each of which corresponding to six minutes of data.

ACPD
13, 10009–10047, 2013

In order to make this data more suitable to the analysis of climate related objectives, a subset of these data is collected in a single daily file, referred to as AIRS Calibration Data Subset (ACDS), also available from the GSFC/DISC. The ACDS contains AIRS, AMSU-A and AMSU-HSB calibration related data, including all spectra between latitudes 50° N to 50° S, where the brightness temperature in the atmospheric window channel at 1231 cm^{-1} (bt1231) is less than 225 K. We refer to these data as Cold Cloud Features (CCF), which are found on average in 2.3 % of the tropical zone. Many CCF are grouped in CCF clusters containing one or more DCC.

3 Deep convective clouds selection and characterization

From all CCF, each day on average 22 000 CCF are found in the tropical zone, 30° S to 30° N. In order to quantify the distance of the cloud tops from the tropopause we use several AIRS channels and channel differences. The brightness temperatures (bt) measured in these channels are denoted by their spectral response function center wavenumbers in cm^{-1}. Thus bt1231, bt900, and bt790 define the brightness temperatures at the shortwave start, the center, and long-wave end of the 11 µm atmospheric window, which extends from about 8.1 µm (1231 cm^{-1}) to 12.7 µm (790 cm^{-1}). The bt1419 refers to the water vapor sounding channel at 1419 cm^{-1}. Under cloud-free tropical conditions this channel sounds near 12 km altitude. We will also use the difference DTW = bt1231 – bt1419, which has typical values in the range of 65 K to 75 K under clear-sky tropical conditions. In the following we first discuss the method that will be used to select cold clouds based on the proximity of their cloud tops to the tropopause. We then discuss the relationship of the selected objects to deep convection or overshooting convection based on simultaneous observations with AMSU-HSB and on results from the literature.

ACPD
13, 10009–10047, 2013

3.1 DCC selection

Conceptually, there are three methods to identify cold clouds near the tropopause, among them: (1) using a fixed brightness temperature threshold, (2) using a threshold based on the difference between a surface channel and a sounding channel, and (3) using a threshold relative to the climatological tropopause temperature.

1. The legacy method in the infrared for the selection of DCC uses a fixed brightness temperature threshold for the broad 11 µm atmospheric window channel, T_{B11}, typically 210 K (Mapes and House 1993; Gettelman et al., 2002). As noted above the 11 µm window actually extends from about 8.1 µm (1231 cm^{-1}) to 12.7 µm (790 cm^{-1}). The properties of the DCC identified by fixed T_{B11} threshold vary with the latitude, longitude and the composition of the cloud top. Figure 1 shows the latitude dependence of the tropical tropopause temperature, T_{Trop}, as a mean over 1981–2010 data from the National Centers of Environmental Prediction (NCEP) Reanalysis (Kalnay et al., 1996, available from NOAA/OAR/ESRL PSD, Boulder, Colorado, USA, http://www.esrl.noaa.gov/psd/). It varies zonally and seasonally from between 193 K to 212 K. In addition, T_{B11} corresponds to the temperature at which the cloud becomes optically thick at 11 µm. From Fig. 1 it is clear that there is no simple relationship between cloud top temperature and the climatological tropopause temperature. Aumann et al. (2011) modeled the tops of cold clouds as uniform slabs of ice clouds using a range of particle sizes and densities at various heights relative to the tropopause, where the cloud properties were fitted to match the observed slope across the 11 µm window. At the center of the 11 µm window these clouds become optically thick at about 20 hPa below the physical cloud top. For a tropical profile at 100 hPa this corresponds to a penetration depth into the physical cloud top of about 1 km, corresponding to about 4 K. This means that the DCC selected with $T_{B11} < 210$ K have clouds tops at 206 K, i.e. they are well below the tropopause, except near 30° N and 30° S.

ACPD
13, 10009–10047, 2013

2. A threshold based on the difference between a surface channel and a sounding channel was first used with T_{B11} and the broad 6.7 μm water channel, $T_{B6.7}$ (e.g. Ackerman 1996; Schmetz et al., 1997). The brightness temperature $T_{B6.7}$ refers to a layer where the atmosphere becomes opaque due to the combined opacity of water vapor or clouds. In the presence of optically thick clouds and without water vapor T_{B11} and $T_{B6.7}$ would be nearly identical. With water vapor, the absorption due to water vapor in the region located between the pressure level at which the cloud becomes optically thick and the tropopause is counteracted by the emission from water vapor above the tropopause in the warmer stratosphere. Historically, clouds with $T_{B11} - T_{B6.7} < 0$ were assumed to overshoot the tropopause (Ackerman 1996). With AIRS data we use the difference between the extremely clear window channel bt1231 and the very strong water vapor channel bt1419, which is conceptually similar to $T_{B11} - T_{B6.7}$, but avoids the ambiguity due to wide bandwidth. Figure 2 illustrates the relationship between the differences DTR = bt900 – T_{Trop} and DTW = bt1231 – bt1419 in a scatter diagram for all CCF collected in September 2002. Overlaid in white are the mean, the 16 % and 84 %-tiles of the distribution function. About 0.6 % of the area of the tropical zone satisfies the condition DTW < 0, but DTR is typically +12 K, i.e. the cloud tops are well below the tropopause. Still, about 30 % of the objects selected using the condition DTW < 0 satisfy the condition DTR < 4 meaning that the physical cloud tops are above the tropopause. We use the condition DTR < 4 K to make an approximate adjustment for the 4 K penetration depth. Typically 0.16 % of the area of the tropical zone is filled with DCC identified by the condition DTW < –4 K, and 80 % of these clouds (0.12 % of the area) have bt1231 lower than the brightness temperature of the climatological tropopause. The mean of the distribution function shown in Fig. 2 reveals an empirical relationship between DTW and DTR, which we use to select DCC based on their proximity to the local tropopause.

3. The third method is based on the threshold relative to the climatological tropopause temperature. Rather than using DTW for the selection of DCC and

ACPD
13, 10009–10047, 2013

making an indirect case for the proximity of the cloud tops to the tropopause, DCC can be identified as clouds where the difference between T_{B11} and T_{Trop} is less than a selected threshold. Gettelman et al. (2002) used the condition $T_{B11} - T_{Trop} < 0$ to identify clouds overshooting the tropopause. Here we use the bt900 $- T_{Trop} < 2$ threshold, in order to account for the penetration depth of the 900 cm^{-1} signal into the cloud top. The drawback of using T_{trop} directly is that it fails to account for local variations of the actual tropopause temperature from the climatological T_{trop}, that correlate with deep convection.

Table 1 summarizes the results of application of three methods of DCC selection described above. The first column in Table 1 denotes the type of the DCC, the second column defined the threshold, e.g. DCC210 is the set of all cold clouds from the tropical zone that satisfy the condition bt900 < 210 K. Cold clouds selected with the DTW < 0 and DTW < −4 K thresholds are referred to as DCCw0 and DCCw4, respectively. We define DTR = bt900 $- T_{Trop}$ to emulate the legacy definition $T_{B11} - T_{Trop}$, but the statistical analysis for the DCCt2 uses 99 km × 23 km threshold to account for the cloud optical depth. The ratio of the count of objects selected by the thresholds divided by the maximum count of possible objects in a given area and multiplied by 100 represents the percent of the area covered by these objects. We identify this ratio with the DCC frequency of occurrence, or simply the DCC frequency. The 3rd through 7th columns present the 10 yr mean DCC frequencies for the entire tropical zone subdivided into day/night and land/ocean.

3.2 DCC selection verification

From the IR data alone we only know the frequency of DCC in the tropical zone as function of the proximity of cloud tops (defined by the unit optical depth at 1231 cm^{-1}) to the tropopause. DCCw0 clouds cover 0.6 % of the tropical zone and about 30 % of them have cloud tops above T_{Trop}. DCCw4 clouds cover 0.16 % of the tropical zone and 80 % (0.12 % of the area of the tropical zone) have cloud tops overshooting the

ACPD
13, 10009–10047, 2013

climatological tropopause. In order to interpret the DCC frequency as the frequency of severe storms, we have to verify that the cold clouds selected with AIRS, using the purely radiometric inequality bt1231 – bt1419 < –4 K, are not simply optically thick ice clouds, but are associated with deep or overshooting convection. For this we use observation with other instruments directly or indirectly in a statistical manner.

For the direct verification we use the set of inequalities derived by Hong et al. (2005) for the three 183 GHz water channels from AMSU-B on NOAA polar orbiters. During September 2002, while AMSU-HSB on EOS Aqua was in operation, 53 % of pixels which were identified as DCCw0 (72 % as DCCw4) using the infrared alone, were identified as microwave deep convection and 22 % (39 % for DCCw4 case) were identified as microwave overshooting convection. Table 2 summarizes this information for the cited and other detection thresholds and also includes results from November 2002 and January 2003 data. For each month about 200 000 DCC210 are identified.

A comparison of the detection frequency of deep convection using other observing systems provides an indirect verification. Hong et al. (2005) used NOAA 15, 16 and 17 AMSU-B 183 GHz channels trained on TRMM data to show that 0.3 % of the area of the tropics is associated with deep convection, 0.08 % of the area is overshooting convection. These frequencies are almost exactly the frequencies expected from our direct verification of DCCw0 using AMSU-HSB on EOS Aqua. Liu and Zipser (2007) used 13.8 GHz Rain Radar (PR) and Visible and Infrared Scanner (VIRS) data from TRMM. They found that in the 20° to 20° S zone 57 % of the clouds that satisfy $T_{B11} < 210$ K, rain was detected by the PR near the surface. This is consistent with our finding that 50 % of the DCC210 are associated with AMSU-HSB deep convection. Young et al. (2012) made use the 95 GHz cloud radar from CloudSat, the lidar from CALIPSO (Cloud-Aerosol Lidar in the A-train) and MODIS data to gain insight into the meaning of the $T_{B11} - T_{B6.7} < 0$ threshold. They concluded that 61 % (55 %) of the objects selected with the $T_{B11} < 210$ K ($T_{B11} - T_{B6.7} < 0$) threshold are associated with deep convection that reaches 14 km altitude, i.e. the base of the Tropopause Transition Layer (TTL). This is consistent with the frequency found using our DCC210 and DCCw0 thresholds.

ACPD
13, 10009–10047, 2013

Figure 3 shows the global distribution of the DCCw0 and DCCw4 for September 2002. There is a high degree of spatial correlation between DCCw0 and DCCw4. This suggests that DCCw4 are tropopause penetrating clouds, which are surrounded by DCCw0 at the center of even larger clusters of CCF.

In the Sect. 4 we analyze trends in the frequency of DCCw0 and DCCw4 in 2002–2012. For consistency with legacy definitions we also evaluate trends for DCC210 and DCC200, which satisfy the simple bt900 < 210 K and < 200 K conditions, respectively. The bt900 – T_{Trop} < 2 K threshold relative to the climatology tropopause temperature defines the least frequent class of DCC, DCCt2.

4 Trend analysis

In the following we illustrate the ten-year trend analysis using the DCCw0. The top panel in Fig. 4 shows the daily DCCw0 fraction for the tropical zone. Each dot represents the day/night averaged area fraction. The same data is shown in the bottom panels, smoothed with a 96-day running mean. The smoothing is used only to better illustrate the seasonal pattern, the data processing uses the daily values. We use 96-day smoothing since it is a multiple of the 16-day EOS Aqua orbit repeat cycle. All data shown in the following are presented after smoothing. The annual variability is clearly seen in the relatively quiet period between 2003 and 2007, thereafter it is overshadowed by ENSO episodes. When the land and ocean area fractions are overlaid (shown in Fig. 5 for the night data), it become apparent that (normalized to area) there are more DCC over land than over ocean. This fact is consistent with the diurnal cycle of precipitation in the tropics (Liu and Zipser, 2005). The frequency of DCC over land has been increasing, while it has been decreasing over ocean. Part of the variability seen in Fig. 5 is seasonal. This variability is removed to determine the anomaly defined as the difference between the daily data and the least-squares-fit of the data to a low order harmonic series. Numerical details of this procedure and the estimation of the anomaly trend and trend uncertainty are given in the Appendix. Figure 6, which

ACPD
13, 10009–10047, 2013

shows the anomalies for DCCw0 identified over land and ocean (heavy trace), confirms the land/ocean frequency anti-correlation ($r = -0.70$). The anomaly trend for ocean is $-0.46 \pm 0.16\,\%\,\mathrm{yr}^{-1}$, for land it is $+1.78 \pm 0.21\,\%\,\mathrm{yr}^{-1}$, where the stated uncertainties correspond to 1σ confidence level. Table 3 lists the anomaly trends and the trend uncertainties for the tropical day/night average, land/ocean, day/night, for the various DCC thresholds matching Table 1. Tables 4 and 5 show the DCCw0 mean frequencies and frequency trends subdivided into four tropical oceans (East Pacific, West Pacific, Indian and Atlantic Ocean) and three land areas (Americas, Africa, and India/Australia). The split of the Pacific into the West and East basin has been done to test whether the DCC trend are different over the so-called ENSO centers of action.

5 Discussion

Before discussing the observed trends, we would like to remind the reader which variables were subjected to the trend analysis: we select cold clouds at/or above the tropopause using the AIRS IR data (Sect. 3). We identify DCC using thresholds relative to bt900, the difference bt1231-bt1419, and the difference between bt900 and climatological tropopause temperature. Of the DCC identified using the infrared alone, 50–75 % are also identified by simultaneous AMSU-HSB measurements as microwave deep convection, and more than 40 % of these DCC match the criteria for microwave overshooting convection. While the trends deduced from the DCC selected using AIRS IR data statistically pertain to deep convection, on a case-by-case basis some fraction of DCC selected using AIRS IR data alone is not associated with deep or overshooting convection. This explains observations by Bedka et al. (2010) and Setvak et al. (2013), who noted that in detailed case studies of cold clouds selected using the MODIS channels M31 and M27, the $T_{\mathrm{m31}} - T_{\mathrm{m27}} < 0$ threshold identifies not only overshooting cloud tops but almost the entire convective anvil cloud.

The changes in the DCC frequency with time, summarized in Table 3, show several interesting features:

ACPD
13, 10009–10047, 2013

5.1 Trends over land and ocean

We find an almost total absence of a trend on a global scale, but strongly anti-correlated trends for land and ocean. Note that while the 10 yr mean frequencies of the DCC differ by almost 2 orders of magnitude, the trends are close, to within a factor of two. We find that the frequency trends are increasing over land and decreasing over ocean independent of the criteria for selection of DCC. The frequency trend nearly cancels for the global average, except for the DCCt2 (tropopause overshooting) group, where the decreasing global trend is marginally significant. DCC correlate with intense precipitation events. The observed tropical zone, land and ocean trends in the DCC frequency are consistent with the WCRP report on trends in global precipitation (2008). That report finds no significant trend in precipitation between 1979 and 2004 and also notes the anti-correlation between land and ocean. The 10 yr time span of the AIRS data is too short to observe the reversal of the observed land/ocean trend for DCC, which is expected based on the precipitation record.

The large magnitude and opposite signs of regional trends rules out instrumental artifacts. But when the trend get closer to zero even small systematic instrument trends have to be taken into consideration. Since DCC are threshold identified, an instrument trend could introduce an artificial trend in the count of DCC. The trend in bt1231 and bt900, which is measured relative to ocean buoys under clear tropical ocean conditions, has been less than $0.01\,\mathrm{K\,yr^{-1}}$ (Aumann et al., 2012). If, due to an instrument trend, the bt900 < 210 K threshold were to change over the ten year to become effectively a bt900 < 211 K threshold, the frequency of DCC would increase from 0.8 % to 0.89 %, i.e. a 10 % increase per degree K. This corresponds to a trend artifact of less than $10 \times 0.01\,\%\,\mathrm{yr^{-1}} = 0.1\,\%\,\mathrm{yr^{-1}}$. Since this effect is smaller than the observed trend uncertainties, it can safely be neglected.

ACPD
13, 10009–10047, 2013

5.2 DCC correlation with ENSO

The frequency anomaly patterns, shown in Fig. 5 for the nighttime data over the Pacific Ocean, and the patterns for DCC determined by other thresholds (not shown), suggest a correlation with the El Niño Southern Oscillation (ENSO). To quantify the correlation we employ the Multivariate ENSO Index (MEI, Wolter and Timlin, 1998), which is often used for the analysis of inter-annual variability and trends in climate studies. The MEI is available as a monthly time series from http://www.esrl.noaa.gov/psd/enso/mei/table.html. It is closely related to the surface temperature anomaly of the Niño34 region in the central Pacific Ocean, normalized to zero mean and unity standard deviation for the values between 1950–1993. The MEI for the past ten years has had a small, but significant negative trend of $-0.13 \pm 0.04\,\mathrm{K\,yr^{-1}}$. Figs. 7 show an overlay of the nighttime ocean and land DCCw0 frequency anomalies and the MEI (heavy trace). The correlation coefficient between DCC and MEI time series is +0.64. For land, the MEI and the DCC frequency are strongly anti-correlated, $r = -0.67$. The observed correlations and anti-correlations result not only from trends, they are also seen in Quasi-Bi-Annual patterns. The correlation between the day ocean DCCw0 anomaly and the MEI is small ($r = +0.25$). This can be explained by the regional analysis. The regional pattern in DCCw0 frequency trends, listed in Tables 3 and 4, are consistent with the classical picture of circulation cells in the tropical zone (Webster, 1983). For the Atlantic Ocean and Indian Ocean the DCCw0 anomaly and MEI is anti-correlated ($r = -0.60$ and $r = -0.63$, respectively), while the correlation is positive ($r = +0.80$) for the Pacific Ocean (Fig. 8). The DCC anomaly trends over Indian and Atlantic oceans have the same sign as tropical land areas (Africa and America), because the main circulation cells related to these oceans originate from Africa and America. The correlation between the MEI and the DCC anomalies points to an interesting perspective of the regional analysis of storms and heavy precipitation in the past, since the SST anomaly in the Niño34 region is available in the form of the extended MEI since 1871 (Wolter and Timlin, 2011).

ACPD
13, 10009–10047, 2013

5.3 DCC correlation with ascending air motion

The relationship between ascending air, clouds and convection is numerically represented in models by the vertical velocity. Bony et al. (2004) suggested using the 500 hPa vertical velocity, ω_{500}, as a proxy for the large-scale vertical motions in the atmosphere. The vertical velocity is calculated daily on a global 2.5° × 2.5° grid by the National Centers for Environmental Prediction (NCEP) Reanalysis. We refer to its value at 500 hPa as ω_{500}. By convention the negative ω_{500} corresponds to ascending motions. In order to test the role of ω_{500} in relation to the DCC frequency anomaly we divide the data into land and ocean areas with negative ω_{500}. Although an ascending air motion does not associate only with DCC, a decrease in the area of negative ω_{500} can generally be interpreted as a decrease in convective cloudiness. For the past ten year on average 75 % of the tropical ocean, 15 % of tropical land area were associated with $\omega_{500} < 0$. Figure 9 shows the anomaly of the daily count (day + night overpasses) of 2.5° cells identified with $\omega_{500} < 0$. The time series over land and ocean are anti-correlated ($r = -0.60$). The fraction of the ocean with $\omega_{500} < 0$ has decreased for ocean at the rate of $-0.33 \pm 0.024\,\%\,\mathrm{yr}^{-1}$, indicating a decrease in convection, while for land it has increased at the rate of $+0.5 \pm 0.05\,\%\,\mathrm{yr}^{-1}$, indicating an increase in convection. Figure 10 shows the overlay of the land (top panel) and ocean (bottom panel) of the DCCw0 anomaly, both day + night averaged, on the $\omega_{500} < 0$ anomaly. The trends in the DCCw0 frequency and the area associated with $\omega_{500} < 0$ are correlated, i.e. not surprisingly the trends in convection and deep convection are correlated. However, the DCCw0 frequency over land increased at the rate of $+1.5 \pm 0.2\,\%\,\mathrm{yr}^{-1}$, three times faster than the area of $\omega_{500} < 0$, which increased at the rate of $+0.5 \pm 0.05\,\%\,\mathrm{yr}^{-1}$. For ocean the DCCw0 decreased at the rate of $-0.73 \pm 0.14\,\%\,\mathrm{yr}^{-1}$, which is twice as fast as the area of $\omega_{500} < 0$ decrease ($-0.33 \pm 0.024\,\%\,\mathrm{yr}^{-1}$).

ACPD
13, 10009–10047, 2013

5.4 Trend balance between tropical land and ocean

The highly significant DCC trends for the tropical oceans are almost exactly counterbalanced (area weighted) by the equally significant, but opposite tropical land trends. Table 3 shows that this balance is independent of the criteria for DCC identification. The anomaly trend for the entire tropical zone, expressed as percentage of the mean, ranges from $+0.1 \pm 0.07\,\%\,\mathrm{yr}^{-1}$ to $+0.038 \pm 0.10\,\%\,\mathrm{yr}^{-1}$ depending on which DCC group is selected. Generally speaking, the near cancelation of the large positive land (25 % of the area of the tropical zone) trend by the negative ocean (75 % of the tropical zone) trend is caused by mass conservation, i.e. an increasing (decreasing) ascent must be balance with increasing (decreasing) descent. However due to the complexity and variability of tropical circulation this general law of balance does not tell us where the anomalous ascend or descend occur. Our study specifically shows the evolution of the anomalies in different regions, which is important for understanding the variability of tropical circulation.

The observation that the increase in the land DCC frequency is counterbalanced by the decrease in the ocean DCC frequency, combined with the regional correlation of the DCC frequency anomaly with the MEI, the correlation of the DCC frequency anomaly with the $\omega_{500} < 0$ anomaly, and the $\omega_{500} < 0$ land/ocean trend anti-correlation suggest a simple interpretation: the observed changes may be part of a decadal variability that shifts the distribution of DCC in the tropics. An association of the changes only with ENSO may be an oversimplification, since the trends of the centers of ENSO action, approximated by the division of the Pacific Ocean into East and West, are almost the same. The increase in the DCC frequency for land has been matched for the past ten years by a decrease for ocean.

Since DCC are associated with intense precipitation, the increase in the frequency of DCC for land results in an increase in precipitation over land, which is counter-balanced by a decrease in precipitation over ocean. This land/ocean balance can be interpreted as evidence for global precipitation being constrained by the energy balance in the

ACPD
13, 10009–10047, 2013

atmosphere (Allan and Soden, 2007). This balance may also be the explanation for the lack of a trend in the frequency of "High Clouds" in the tropical zone reported by Wylie et al. (2005). In the DCCt2 group, which significantly overshoots the tropopause and as such is interesting due to the correlation between overshooting convection and severe storms, the decreasing global trend is not 2σ significant.

5.5 Extreme events

Table 2 shows that the tighter DCC selection thresholds identify fewer DCC, which are more likely associated with microwave overshooting convection, which in turn is presumed to be associated with more severe storms. From Table 3 we also note that the less frequent DCC (DCCt2 and DCCw4 types) show consistently larger decreases in frequency for ocean and larger increases over land than the less frequent ones (DCCw0 and DCC210 types). We also note that the condition $\omega_{500} < 0$ is associated with convection, while DCC are associated with deep convection. The two quantities are correlated, which may not be too surprising, but the rate of change in the DCC (convection extremes!) for land and ocean is a factor of 2–3 times faster than the change in $\omega_{500} < 0$ (mean circulation), as discussed in Sect. 5.2. This finding fits into a framework of how weather extremes respond to climate change (c.f. Allen and Ingram, 2002; Emori and Brown, 2005).

6 Summary

The difference between the brightness temperature measured with AIRS in the 1231 cm^{-1} atmospheric window channel and the brightness temperature in the strong water vapor absorption line at 1419 cm^{-1} is a measure of the proximity of the clouds tops to the tropopause. This difference and other thresholds are used to identify DCC. DCC referred to a DCCw4 cover 0.16 % of the tropical zone and have cloud tops at or above the tropopause. This is confirmed by simultaneous observations with the AMSU-

ACPD
13, 10009–10047, 2013

HSB 183 GHz water vapor channels, which identify about 70 % of the DCCw4 as deep convective, about 40 % as overshooting. The association of DCC with severe storms has been documented in the literature using infrared, microwave and rain radar studies. In the past ten years the frequency of DCC in the tropical zone has changed insignificantly, but it decreased by about 1 % yr^{-1} for the tropical ocean, while it increased about +2 % yr^{-1} for tropical land. This pattern of essentially zero trend for the tropical zone, but opposite land/ocean trends, is consistent with measurements of global precipitation seen in 25 yr of data. However, the 10 yr time span of the AIRS data is too short to observe the reversal of the observed land/ocean trend for DCC, which is expected based on the precipitation record. The frequency of DCC observed over ocean and over land serves as a tracer of tropical circulation patterns. To first order, the changes in the frequency of DCC are correlated with the change in the fraction of land and ocean areas associated with ascending and descending air motion, defined by vertical speed ω at 500 hPa, ω_{500}. However, changes in the DCC frequency for land and ocean are a factor of 2–3 time faster than the change in ω_{500}. The correlation of the DCC frequency with the ENSO index and the land/ocean anti-correlation of the trend in the area associated with $\omega_{500} < 0$ suggest that the observed changes are part of a decadal variability, which results in small shifts in the tropical circulation pattern, but cancel globally on a ten year time scale. The correlation and anti-correlations of the DCC frequency anomaly with MEI and the association of DCC with storms and heavy precipitation points to an interesting perspective of the regional analysis of past events, since the SST anomaly in the Nino34 region is available in the form of the extended MEI since 1871. Depending on the selected threshold, the frequency of DCC in the tropical zone decreases from 0.8 % of 0.06 % area, and the least frequent, more extreme DCC show the largest trend in frequency, increasing over land, decreasing over ocean. This finding fits into the framework of how weather extremes respond to climate change.

ACPD
13, 10009–10047, 2013

Anomaly trend evaluation

We use the time series of the daily fraction of DCCw0 for tropical land to illustrate the anomaly trend analysis procedure. The left panel of Fig. A1 shows the daily DCCw0 frequency. The mean of this time series is 0.0092 with a standard deviation $\sigma = 0.0028$, 5 % of the data exceed the mean $+2\sigma$. The daily variability is substantial, but the character of the noise appears to be to first order Gaussian. The noise in the daily measurements hides an annual variability. To illustrate this, the right panel of Fig. A1 shows the same data as the left panel, but the data are smoothed with a 3 months running mean (we use 96 days, because it is a multiple of the EOS Aqua 16 day orbit repeat cycle). The smoothing reveals a pronounced annual variability, which almost dominates a more complicated pattern starting in 2008. A simple linear fit through the data yields a slope of $+0.00014\,\mathrm{yr}^{-1}$ with a one-sigma slope uncertainty of $0.000022\,\mathrm{yr}^{-1}$. The slope is eight times larger than the uncertainty. Expressed as percentage of the mean (0.0092) the trend is $+1.75 \pm 0.22\,\%\,\mathrm{yr}^{-1}$, where the trend uncertainty is one sigma confidence.

Visual inspection of Fig. A1 may cast some doubt on the validity of the trend and trend uncertainty derived from the linear analysis. To get a better estimate we use anomaly trend analysis. For this purpose we fit the data to a low order harmonic function to X, which fits the seasonal variability, but keeps all lower frequency terms.

$$X_{\mathrm{fit}} = M_{\mathrm{o}} + \sum_{n=1.6} [a \sin(2\pi n t) + b \cos(2\pi n t)],$$

where $t = (\mathrm{J} - \mathrm{J_o})/365.24$ and $\mathrm{J_o}$ is the Julian day number of the center of the time series. The choice of $n = 1, \ldots, 6$ adequately fits the seasonal variability and is not critical. The anomaly time series $A(t) = (x - X_{\mathrm{fit}})$ retains the linear trend of the original time series, and the character of the noise, with the annual and seasonal variability and the mean being removed. By definition $A(t)$ has zero mean. The linear trend of $A(t)$ is referred to the anomaly trend. Expressed as percentage of the mean (0.0092) the

ACPD
13, 10009–10047, 2013

anomaly trend with 1σ confidence is $+1.75 \pm 0.15\,\%\,yr^{-1}$. In this example the trend did not change. The 1σ trend uncertainty decreased significantly compared to the simple linear fit to the data, because of the removal of seasonal variability, which contributed to the variance of the original data.

Acknowledgements. The research described in this paper was carried out at the Jet Propulsion Laboratory, California Institute of Technology, under a contract with the National Aeronautics and Space Administration. Sergio Machado and Scott Hannon of UMBC provided support with model calculations. We are grateful for the long-term support of Ramesh Kakar, Aqua Program Scientist at NASA HQ.

References

Ackerman, S. A.: Global satellite observations of negative brightness temperature differences between 11 and 6.7 microns, J. Atmos. Sci., 53, 2803–2812, 1996.

Adler, R. F. and Fenn, D. D.: Thunderstorm intensity as determined from satellite imagery, J. Appl. Meterrol, 18, 502–517, 1979.

Alcala, C. M. and Dessler, A. E.: observations of deep convection in the tropics using the Propical Rainfall Measuring Mission (TRMM) precipitation radar, J. Geophys. Res., 107, 4792, doi:10.1029/2002JD002457, 2002.

Allan, R. P. and Soden, B. J.: Large discrepancy between observed and simulated precipitation trends in the ascending and descending branches of the tropical circulation, Geophys.Res. Lett., 34, L18705, doi:10.1029/2007GL031460, 2007.

Aumann, H. H., Chahine, M. T., Gautier, C., Goldberg, M., Kalnay, E., McMillin, L., Revercomb, H., Rosenkranz, P. W., Smith, W. L., Staelin, D. H., Strow, L., and Susskind, J.: AIRS/AMSU/HSB on the Aqua Mission: design, science objectives, data products and processing systems, IEEE T. Geosci. Remote, 41, 253–264, 2003.

Aumann, H. H., Broberg, S., Elliott, D., Gaiser, S., and Gregorich, D.: Three years of Atmospheric Infrared Sounder radiometric calibration validation using sea surface temperatures, J. Geophys. Res.-Atmos., 111, D16S90, doi:10.1029/2005JD006822, 2006.

Aumann, H. H., DeSouza-Machado, S. G., and Behrangi, A.: Deep convective clouds at the tropopause, Atmos. Chem. Phys., 11, 1167–1176, doi:10.5194/acp-11-1167-2011, 2011.

ACPD
13, 10009–10047, 2013

Aumann, H. H., Elliott , D., and Strow, L. L.: Validation of the Radiometric Stability of the Atmospheric Infrared Sounder, Proc. SPIE Optics and Photonics Conference, San Diego, August 2012, Session 8510, Earth Observing System XVII, edited by: Buttler, J., Xiong, X., and Gu, X., 2012.

Bedka, K., Brunner, J., Dworak, R., Feltz, W., Otkin, J., and Greenwald, T.: Objective satellite-based overshooting top detection using infrared window channel brightness temperature gradients, J. Appl. Meteorol. Clim., 49, 181–202, doi:10.1175/2009JAMC2286.1, 2010.

Emori, S. and Brown, S. J.: Dynamic and thermodynamic change in mean and extreme precipitation under changed climate, Geophys. Res. Lett., 32, L17706, doi:10.1029/2005GL023272, 2005.

Gettelman, A., Salby , M. L., and Sassi, F.: Distribution and influence of convection in the tropical tropopause region, J. Geophys. Res., 107, ACL 6-1–ACL 6-12, doi:10.1029/2001JD001048, 2002.

Gettelman, A., Birner, T., Eyring, V., Akiyoshi, H., Bekki, S., Brühl, C., Dameris, M., Kinnison, D. E., Lefevre, F., Lott, F., Mancini, E., Pitari, G., Plummer, D. A., Rozanov, E., Shibata, K., Stenke, A., Struthers, H., and Tian, W.: The Tropical Tropopause Layer 1960–2100, Atmos. Chem. Phys., 9, 1621–1637, doi:10.5194/acp-9-1621-2009, 2009.

Fueglistaler, S., Dessler, A. E., Dunkerton, T. J., Folkins, I., Fu, Q., and Mote, P. W.: Tropical tropopause layer, Rev. Geophys., 47, RG1004, doi:10.1029/2008RG000267, 2009.

Hong, G., Heygster, G., Miao, J., and Kunzi, K.: Detection of tropical deep convective clouds from AMSU-B water vapor channels measurements, J. Geophys. Res., 110, D05205, doi:10.1029/2004JD004949, 2005.

Janowiak, J. E. and Arkin, P. A.: Rainfall variations in the tropics during 1986–1989, as estimated from observations of cloud-top temperatures, J. Geophys. Res., 96, Supplement, 3359–3373, 1991.

Joyce, R. and Arkin, P. A.: Improved estimates of tropical and subtropical precipitation using the GOES Precipitation Index, J. Atmos. Ocean. Tech., 10, 997–1011, 1997.

Kalney, E., Kanamitsu, M., Kistler, R., Collins, W., Deaven, D., Gandin, L., Iredell, M., Saha, S., White, G., Woollen, J., Zhu, Y., Leetmaa, A., Reynolds, R., Chelliah, M., Ebisuzaki, W., Higgins, W., Janowiak, J., Mo, K. C., Ropelewski, C., Wang, J., Jenne, R., and Joseph, D.: The NCEP/NCAR 40 year reanalysis project, B. Am. Meteor. Soc., 77, 437–471, 1996.

Lambrigtsen, B. H. and Calheiros, R. V.: The Humidity Sounder for Brazil – an international partnership, IEEE T. Geosci. Remote, TGARS, 41, 352–361, 2003.

ACPD
13, 10009–10047, 2013

Lambrigtsen, B. and Lee, S. Y.: Coalignment and synchronization of the AIRS instrument suite, IEEE T. Geosci. Remote, 41, 343–351, 2003.
Liu, C. and Zipser, E. J.: Global distribution of convection penetrating the tropical tropopause, J. Geophys. Res., 110, D23104, doi:10.1029/2005JD006063, 2005.
Liu, C. and Zipser, E. J.: Diurnal cycles of precipitation, clouds and lightning in the tropics from 9 years of TRMM observations, Geophys. Res. Lett., 35, L04819, doi:10.1029/2007GL032437, 2008.
Liu, C., Zipser, E. J., and Nesbitt, S.: Global distribution of tropical deep convection: different perspectives from TRMM infrared and radar data, J. Climate, 20, 489–503, 2007.
Reynolds, D. W.: Observations of damaging hailstorms from geosynchronous satellite digital data, Mon. Weather Rev., 108, 337–348, 1980.
Schmetz, J., Tjemkes, S. A., Gube, M., and Van De Berg, L.: Monitoring deep convection and convective overshooting with METEOSAT, Adv. Space Res., 19, 433–441, 1997.
Setvak, M., Lindsey, D. T., Rabin, R. M., Wang, P. K., and Demeterova, A.: Indication of water vapor transport into the lower stratosphere above midlatitude convective storms: Meteosat Second Generation satellite observations and radiative transfer simulations, J. Atmos. Res., 89, 170–180, 2008.
Setvak, M., Bedka, K., Lindsey, D., Sokol, A., Charvat, Z., Staska, P., and Wang, P.: A-Train observations of deep convective storm tops, J.Atmos. Res., 123, 229–248, doi:10.1016/j.atmosres.2012.06.020, 2013.
Sherwood, S. and Dessler, A.: On the control of stratospheric humidity, Geophys. Res. Lett., 27, 677–680, 2000.
Webster, P. J.: Large-scale structure of the tropical atmosphere, in: General Circulation of the Atmosphere, edited by: Hoskins, B. J. and Pearce, R. P., Academic Press, London, 235–275, 1983.
WCRP report on Global Precipitation, WCRP-128, WMP/TD-No. 1430, 2008.
Wolter, K. and Timlin, M. S.: Measuring the strength of ENSO events – how does 1997/98 rank?, Weather, 53, 315–324, 1998.
Wolter, K. and Timlin, M. S.: El Ni no/Southern Oscillation behaviour since 1871 as diagnosed in an extended multivariate ENSO index (ME I.ext), Int. J. Climatol., 31, 1074–1087, doi:10.1002/joc.2336, 2011.
Wylie, D., Jackson, D. J., Menzel, W. P., and Bates, J. J.: Trends in high and low clouds from the analysis of 20 years of HIRS and ISCCP data, J. Climate, 18, 3021–3031, 2005.

ACPD
13, 10009–10047, 2013

Young, A., Bates, J. J., and Curry, J. A.: Complementary use of passive and active remote sensing for the detection of penetrating convection from CloudSat, Calypso and Aqua MODIS, J. Geophys. Res., 117, D13205, doi:10.1029/2011JD016749, 2012.

ACPD
13, 10009–10047, 2013

Table 1. Percent of DCC identified with various IR brightness temperature thresholds and differences, segregated by surface type and time of day, from AIRS data in 2002–2012.

	Threshold	Tropical zone	Ocean day	Ocean night	Land day	Land night
DCC210	bt900 < 210 K	0.800	0.557	0.650	0.932	1.09
DCCw0	bt1231 – bt1419 < 0	0.644	0.501	0.629	0.847	1.01
DCCw4	bt1231 – bt1419 < -4	0.158	0.107	0.184	0.235	0.165
DCC200	bt900 < 200 K	0.140	0.092	0.161	0.197	0.139
DCCt2	bt900 – $T_{\mathrm{Trop}} < 2$	0.061	0.031	0.070	0.072	0.130

ACPD
13, 10009–10047, 2013

Table 2. Percent of DCC identified in the IR with AMSU-HSB deep convection and overshooting convection for September 2002, November 2002 and January 2003.

	Percent AMSU-HSB deep convection			Percent AMSU-HSB overshooting convection		
	Sep	Nov	Jan	Sep	Nov	Jan
DCC210	48	47	46	20	18	17
DCCw0	53	50	50	22	20	20
DCCw4	72	68	69	39	35	36
DCC200	67	66	64	38	32	31
DCCt2	71	72	77	45	43	49

ACPD
13, 10009–10047, 2013

Table 3. Summary of trends and trend uncertainties in $\%\,yr^{-1}$ units.

	Threshold	Tropical zone	Ocean day	Ocean night	Land day	Land night
DCC210	bt900 < 210 K	+0.042 ± 0.12	−0.72 ± 0.17	−1.20 ± 0.17	+1.82 ± 0.22	+1.86 ± 0.24
DCCw0	bt1231 − bt1419 < 0	+0.038 ± 0.10	−0.46 ± 0.16	−1.01 ± 0.16	+1.73 ± 0.21	+1.78 ± 0.21
DCCw4	bt1231 − bt1419 < −4	+0.15 ± 0.17	−0.82 ± 0.27	−1.30 ± 0.25	+2.75 ± 0.33	+2.03 ± 0.32
DCC200	bt900 < 200 K	−0.46 ± 0.21	−1.83 ± 0.32	−2.04 ± 0.30	+2.55 ± 0.36	+1.89 ± 0.36
DCCt2	bt900 − T_{Trop} < 2	−0.58 ± 0.29	−2.41 ± 0.47	−2.13 ± 0.40	+2.35 ± 0.53	+2.51 ± 0.49

ACPD
13, 10009–10047, 2013

Table 4. Trends for tropical oceans.

	West Pacific 120° E–200° E	East Pacific 200° E–280° E	Indian Ocean 30° E–120° E	Atlantic Ocean 280° E–30° E
DCCw0 trend [% yr^{-1}]	−1.79 ± 0.27	−1.51 ± 0.35	+1.05 ± 0.29	+1.71 ± 0.39
Mean DCCw0 frequency [%]	1.04	0.29	0.78	0.24
Relative area	28 %	27 %	25 %	20 %
	−21 ± 2	−49 ± 3		

ACPD
13, 10009–10047, 2013

Table 5. Trends for tropical lands.

	America	Africa	India/Australia
DCCw0 trend [% yr^{-1}]	$+0.76 \pm 0.029$	$+1.18 \pm 0.022$	$+3.15 \pm 0.030$
Mean DCCw0 frequency [%]	1.16	0.849	0.862
Relative area	28 %	34 %	37 %

ACPD
13, 10009–10047, 2013

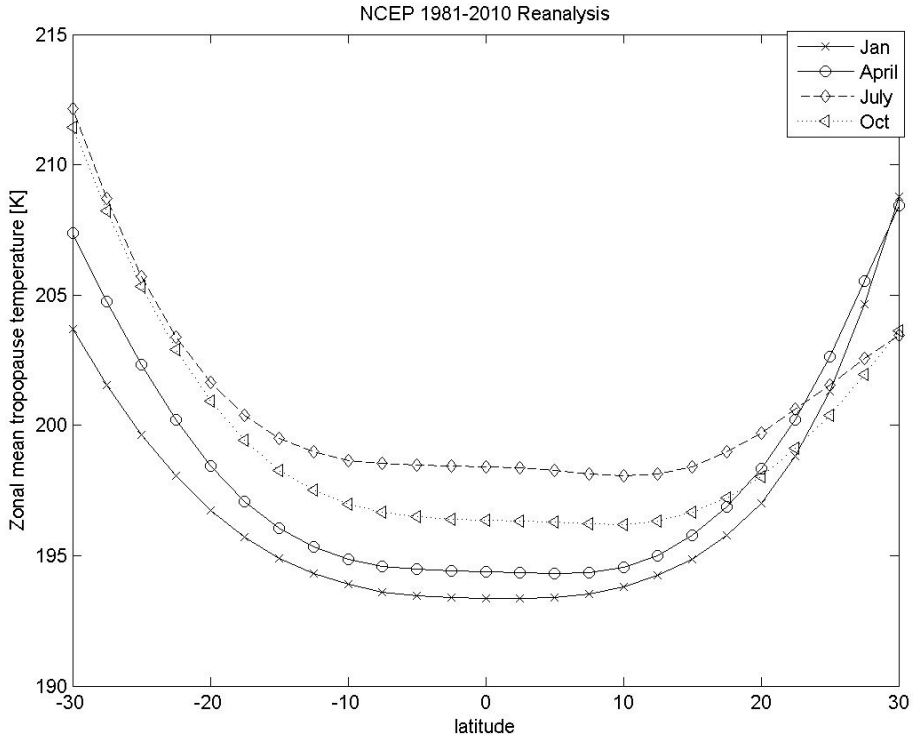

Fig. 1. Latitude dependence of the tropical tropopause temperature based on the NCEP 1981–2010 Reanalysis.

ACPD
13, 10009–10047, 2013

Clouds in the tropical zone from ten years of AIRS data

H. H. Aumann and A. Ruzmaikin

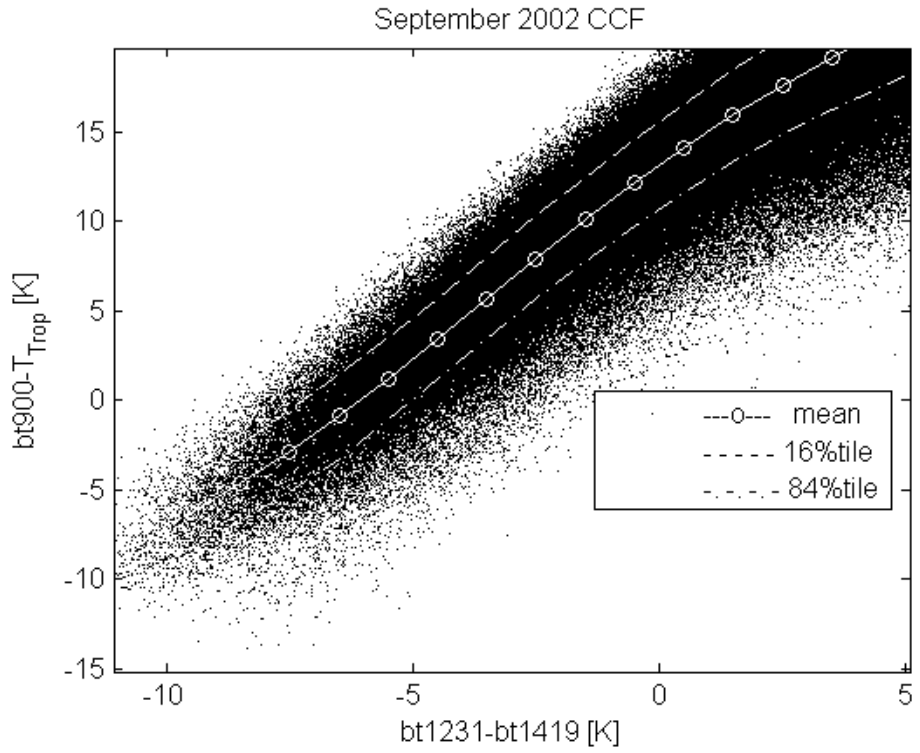

Fig. 2. Scatter diagram DTW versus DTR for high clouds identified within 20 K of T_{Trop}.

ACPD
13, 10009–10047, 2013

Clouds in the tropical zone from ten years of AIRS data

H. H. Aumann and A. Ruzmaikin

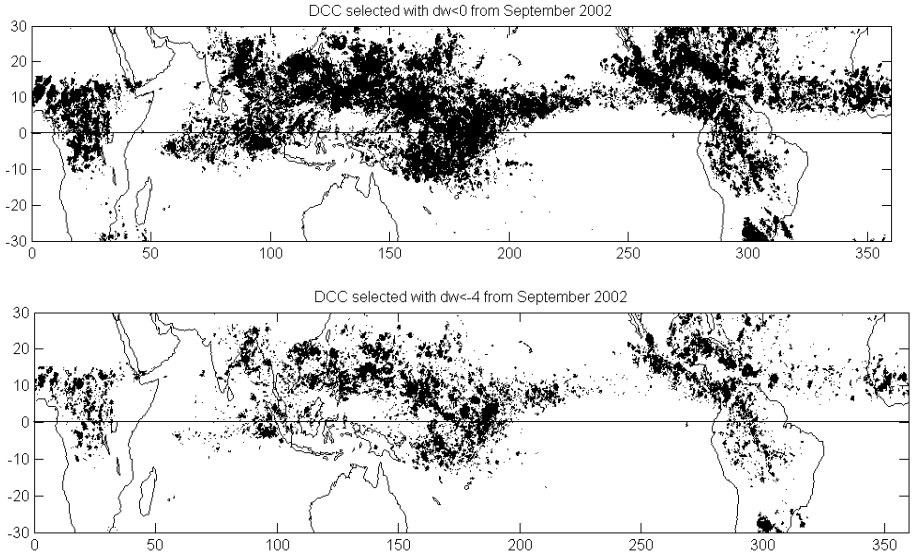

Fig. 3. Top panel: CCF that satisfy the condition DTW < 0. Bottom: CCF that satisfy the condition DTW < −4.

ACPD
13, 10009–10047, 2013

Clouds in the tropical zone from ten years of AIRS data

H. H. Aumann and A. Ruzmaikin

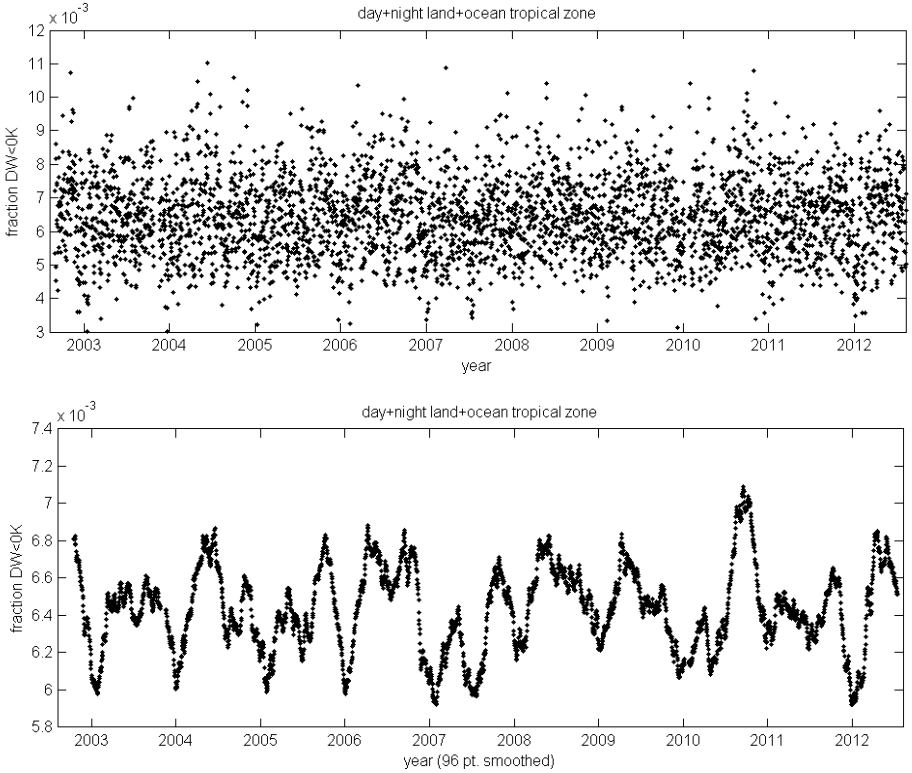

Fig. 4. The daily DCCw0 fraction for the tropical zone. Top: daily points. Bottom: the same points smoothed with 96 day running mean.

ACPD
13, 10009–10047, 2013

Clouds in the tropical zone from ten years of AIRS data

H. H. Aumann and A. Ruzmaikin

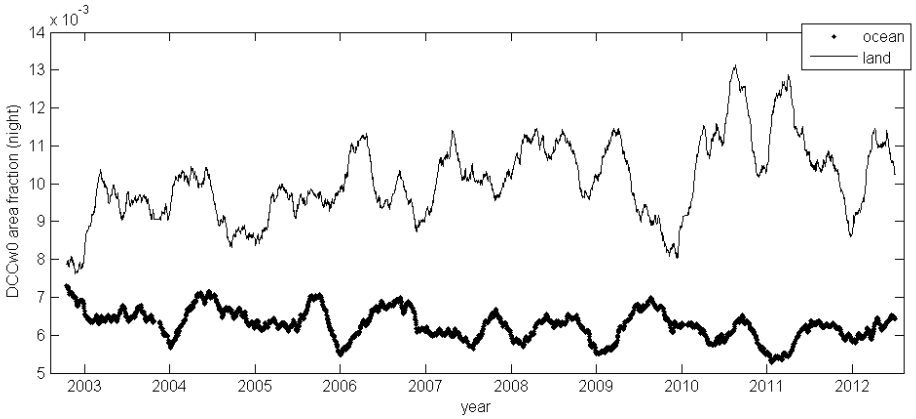

Fig. 5. The night land (solid) and ocean (bold trace) DCCw0 area fractions as function of time.

ACPD
13, 10009–10047, 2013

Clouds in the tropical zone from ten years of AIRS data

H. H. Aumann and A. Ruzmaikin

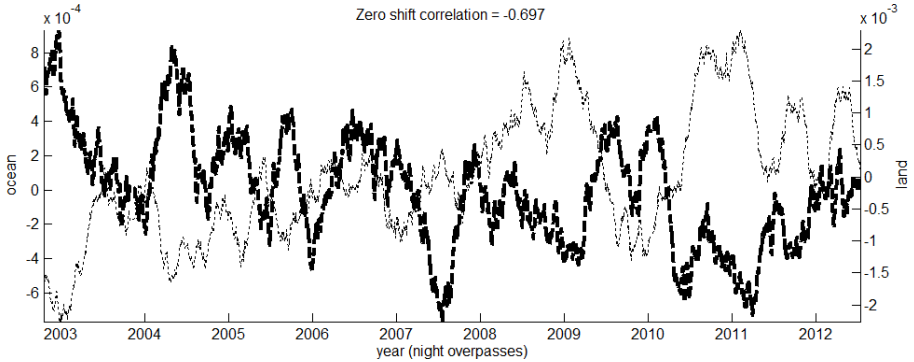

Fig. 6. DCCw0 fraction anomalies of the night overpass data shown in Fig. 5. Bottom: DCCw0 fraction anomalies of the day overpass data. The bold trace refers to ocean; the light trace is for land.

ACPD
13, 10009–10047, 2013

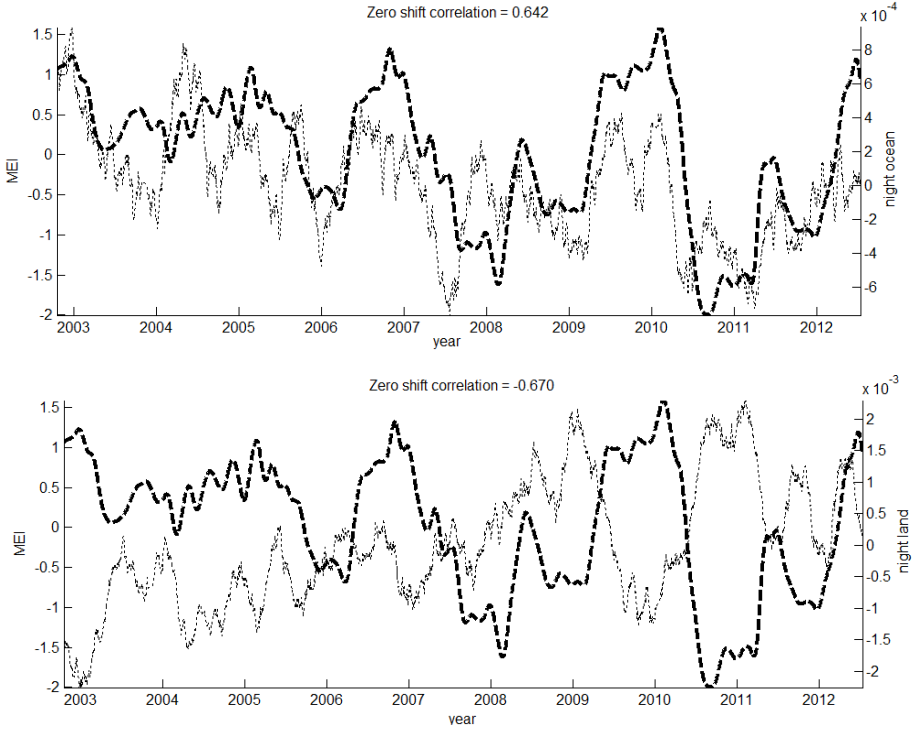

Fig. 7. The DCCw0 anomaly (light trace) and the MEI (heavy trace). Top panel presents ocean night. Bottom panel presents land night.

ACPD
13, 10009–10047, 2013

Clouds in the tropical zone from ten years of AIRS data

H. H. Aumann and A. Ruzmaikin

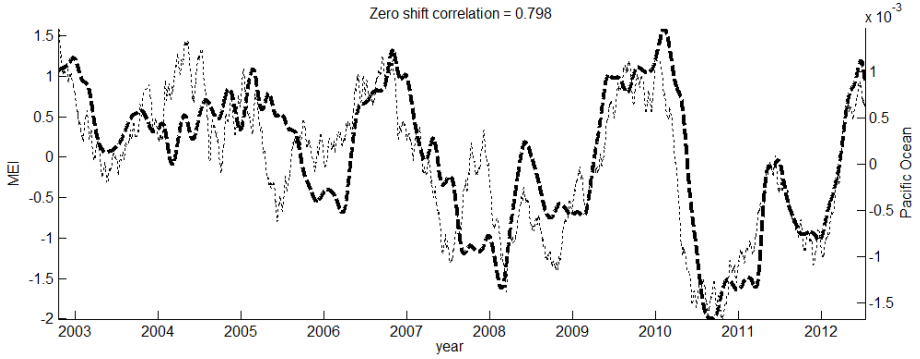

Fig. 8. The DCCw0 anomaly for averaged day/night over Pacific Ocean and the MEI (heavy trace).

ACPD
13, 10009–10047, 2013

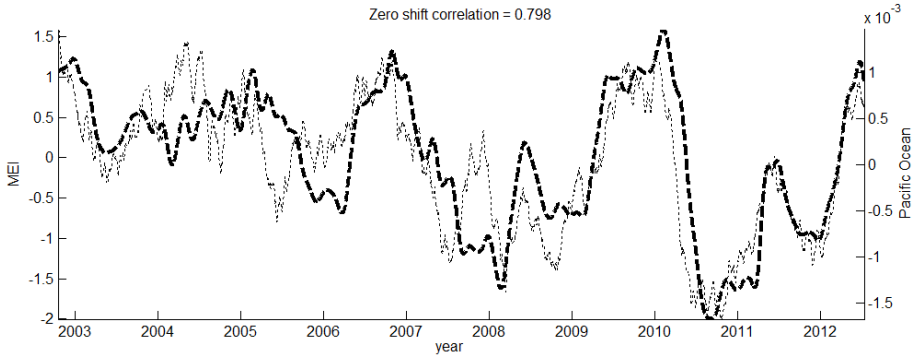

Fig. 9. Anomalies of the daily (day + night overpasses) count of the 2.5° cells identified with $\omega_{500} < 0$ for ocean (bold) and land.

ACPD
13, 10009–10047, 2013

Clouds in the tropical zone from ten years of AIRS data

H. H. Aumann and A. Ruzmaikin

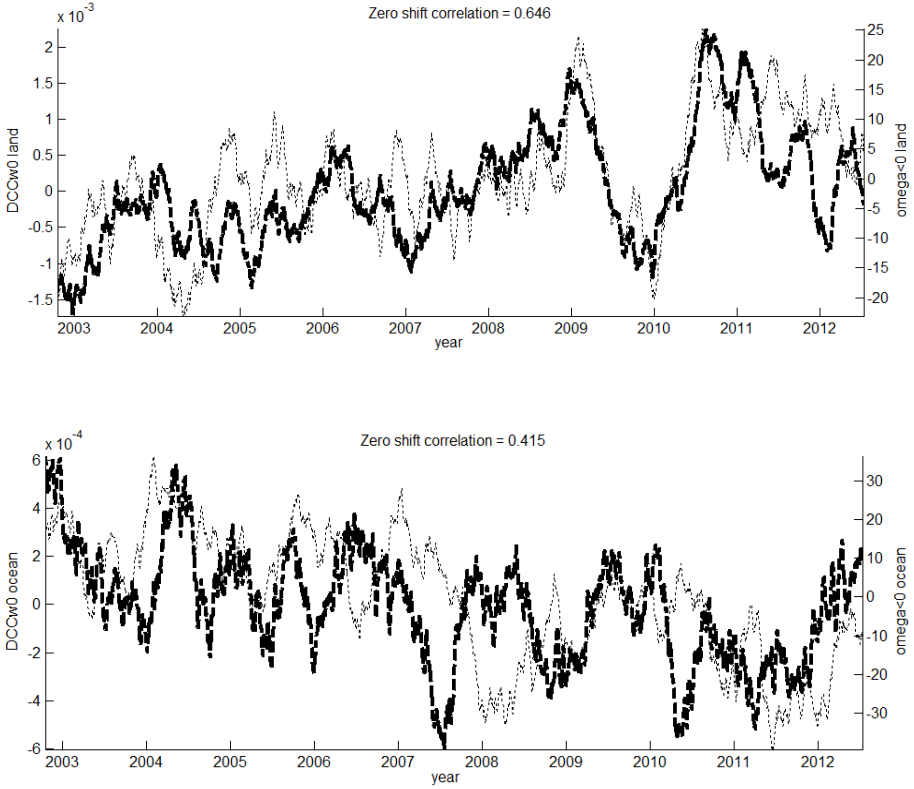

Fig. 10. The land (top panel) and ocean (bottom panel) of the DCCw0 anomaly compared with the $\omega_{500} < 0$ anomaly.

ACPD
13, 10009–10047, 2013

Clouds in the tropical zone from ten years of AIRS data

H. H. Aumann and A. Ruzmaikin

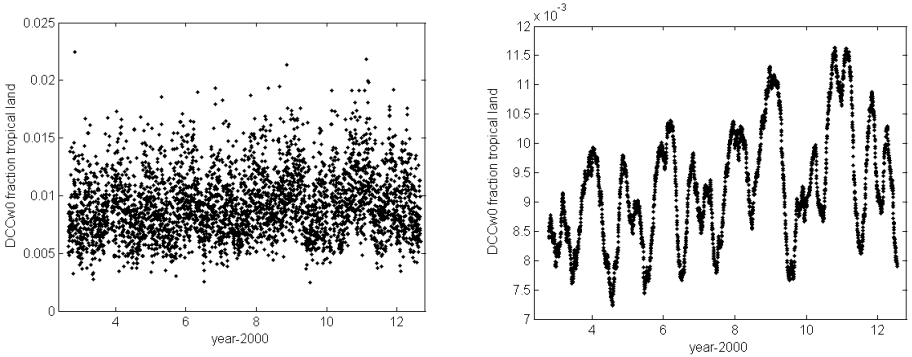

Fig. A1. The left panel shows the day/night averaged daily faction of tropical land associated with DCCw0. The right panel shows the same data, but smoothed with a 96 day running average.

ACPD
13, 10009–10047, 2013